Arch Appl Mech (2016) 86:21–38
DOI 10.1007/s00419-015-1099-z

SPECIAL

Hyung-Jun Chang · Nicolas M. Cordero · Christophe Déprés · Marc Fivel · Samuel Forest

Micromorphic crystal plasticity versus discrete dislocation dynamics analysis of multilayer pile-up hardening in a narrow channel

Received: 2 June 2015 / Accepted: 26 October 2015 / Published online: 2 January 2016
© Springer-Verlag Berlin Heidelberg 2015

Abstract Size effects in the mechanical behavior of multilayer pile-ups embedded in channel microstructures are investigated in terms of work-hardening, plastic slip and geometrically necessary dislocations (GND) distributions. The mechanical responses with various channel sizes are computed by three-dimensional discrete dislocation dynamics (DDD), micromorphic crystal plasticity (Microcurl) and field dislocation mechanics (FDM). The analysis is first limited to single slip with a slip plane perpendicular to the channel walls. In DDD simulations, it is found that the overall work-hardening is strongly dependent on distance between neighbor slip layers. The size dependence disappears when the neighbor layers are close enough to interact with each other. It is confirmed by direct comparison between DDD simulations and two analytical expressions derived from simplified model of multilayer pile-ups. Distributions of slip and GNDs are presented and analyzed for various channel sizes. The cases of inclined slip plane and of double slip systems in a channel are also considered and investigated. The two alternative crystal plasticity theories, Microcurl and FDM, are then found to reproduce the results of DDD. In particular, quantitative correspondence is found between the Microcurl and DDD results.

Keywords Dislocation dynamics · Strain gradient plasticity · Crystal plasticity · Micromorphic continuum · Dislocation pile-up · Field dislocation mechanics · Kinematic hardening

1 Introduction

Dislocation pile-ups are believed to belong to the essential ingredients accounting for size effects since Hall [39] and Petch [53] analyses. Pile-ups at boundaries and their induced stress field tend to restrict further dislocation motion, giving rise to extra work-hardening and size effect. More generally, the constraining role of boundaries related to pile-up formation is responsible for many size effects in crystal plasticity. Understanding and modeling size effects motivated most of the recent works on enhanced crystal plasticity formulations. For example, Acharya and Bassani [1] have incorporated plastic strain gradient directly into hardening description, while Fleck and Hutchinson [29] have used the plastic strain gradient to motivate a non-local continuum formulation involving higher-order stresses. Gurtin [37,38] proposed an approach in which gradient of plastic

H.-J. Chang · N. M. Cordero · S. Forest (✉)
MINES ParisTech, Centre des Matériaux, UMR CNRS 7633, BP 87, 91003 Evry, France
E-mail: samuel.forest@ensmp.fr

C. Déprés
SYMME, Univ. Savoie Mt Blanc, 74000 Annecy, France

M. Fivel
SIMAP GPM2, CNRS, Univ Grenoble Alpes, 38000 Grenoble, France

deformation and related microstresses were introduced. Arsenlis and Parks [3] included a parameter related to the density of geometrically necessary dislocations (GND). Generalized constitutive laws are proposed in [65] to embed dislocations and disclinations in the continuum theory.

Recently, two alternative models, field dislocation mechanics (FDM) and micromorphic crystal plasticity (Microcurl), have been proposed. The FDM incorporates average dislocation densities, statistically stored dislocations (SSDs) and GNDs. The GND density in the model describes extra plastic distortion [54,55]. One-dimensional FDM simulations were sufficient to reproduce size-dependent material behavior of aluminum compounds [63]. The micromorphic continuum-based model [20] introduces a plastic microdeformation tensor to overcome some limitations of existing strain gradient plasticity theory, as illustrated in [31,32,69]. In the latter references, the linear relationship between higher-order stresses and the GND tensor used in standard strain gradient plasticity was shown to lead to physically unrealistic scaling behavior in the response of laminates under shear. The micromorphic model provides more degrees of freedom for the description of size-dependent work-hardening and yield strength. Simplified and computationally effective micromorphic models to describe strain gradient plasticity were recently proposed in [67,68] based on the micromorphic approach.

The relevance of generalized continuum approaches will ultimately be decided through comparison between predictions of the various models and experiments [30,34]. However, detailed comparison with discrete dislocation dynamics (DDD) is also useful in assessing the formulations, because motion of dislocation ensembles computed by the DDD gives rise to intrinsic size-dependent responses [2,12,49,52]. Such comparisons started to be carried out by Bassani et al. [9]. Several alternative formulations were evaluated by DDD simulations [6,11,60,70,71]. These studies have been, however, supported only by two-dimensional DDD computations [16–18,60], so that 3D validations still remain seldom. Such a 3D validation was performed in [61] but limited to classical continuum crystal plasticity. A first comparison between 3D DDD and the Microcurl model was performed in [13] to investigate strain localization phenomena at hard particles in a single crystal.

Three-dimensional DDD deals with realistic physical phenomena resulting from the collective motion of dislocations that curve and intersect. It is expected to provide full description of physics-based crystal plasticity. For instance, only three-dimensional computations can provide line tension-induced dislocation motion and relaxation due to extension of screw dislocations [60]. Up to now, several codes for the three-dimensional DDD have been developed [36,44,57,66,72] and they were applied to a wide range of dislocation-related problems [24,28,41,44,46,59].

Another method for investigation of pile-ups used in the present work is the analytical description based on continuum dislocation theory. Earliest analytical investigations derived by Eshelby [26] have been used as an evidence of the Hall–Petch effect. As a matter of fact, the analytical description displays some limitations to handle general problems of pile-ups due to multiple interactions between dislocations. According to Chou and Li [15], fully analytical solution is available only for single-layer pile-ups in a homogeneous medium. Recently, however, several theoretical expressions for multilayer pile-ups have been derived from reasonable assumptions [7,23,33,42,58] and incorporated into multiscale homogenization schemes [10,19]. For instance, Mura [33] has suggested a simple solution for multilayer pile-ups without consideration of the interaction between neighboring slip layers, while Déprés [23] has incorporated the latter effect in an explicit formula to be discussed in this work. Other asymptotic solutions of pile-ups of infinite walls of edge dislocations were recently analyzed in [8,35,47,56].

In the present work, size effects induced by multilayer pile-ups are investigated in terms of slip and GND distributions and associated work-hardening using the DDD, Microcurl and FDM simulations and two analytical approaches. Stacked double-ended pile-ups of edge dislocations in channel shape volume are considered as a first step in three-dimensional DDD analysis. In addition, pile-ups on inclined slip planes and double slip systems are analyzed. The DDD simulation provides quasi-static dislocation distributions at given loading steps. Then, post-processing of the dislocation distributions deliver slip and GND distributions and related work-hardening. These mechanical responses obtained by DDD are analyzed in terms of channel size effect and compared with results of analytical approaches, Microcurl and FDM simulations both qualitatively and quantitatively.

In particular, the presented DDD simulations show that the distance between neighboring slip planes considered as an internal length in the physical model is an important ingredient to determine size dependence of work-hardening. The size effect is shown to vanish for short enough internal lengths for the dislocations to feel the additional stresses induced by neighboring pile-ups. This effect is accounted for by the DDD simulations and analytical expressions suggested by Mura and Déprés [23,33]. The comparisons provide key

ideas to explain the influence of the internal length on size dependence of work-hardening, as discussed in the present work.

Then, the relevance of Microcurl and FDM models is evaluated from the DDD results. The Microcurl model provides the slip distribution and work-hardening at various channel sizes as in DDD simulations. The intrinsic length of the Microcurl model is identified from direct and quantitative comparisons with the results of DDD simulations. Furthermore, Taupin et al. [63] have predicted GND distribution induced by pile-ups using one-dimensional FDM simulations. Their predictions are introduced here for comparison with results of DDD. Finally, the physical meaning of the intrinsic lengths of the two models, Microcurl and FDM, is discussed.

In the following, first-, second- and third-rank tensors are denoted by $\underline{\boldsymbol{u}}$, $\underset{\sim}{\boldsymbol{\chi}}$ and $\underline{\underline{\boldsymbol{\epsilon}}}$, respectively. The double contraction of two second-order tensors is $\underset{\sim}{\boldsymbol{a}} : \underset{\sim}{\boldsymbol{b}} = a_{ij}b_{ij}$, where repeated indices are summed. The theories and computations are presented within the small strain framework. An extension of the Microcurl model to large deformations can be found in [4]. The curl operator applied to a second-rank tensor is defined in this work as

$$\operatorname{curl} \underset{\sim}{\boldsymbol{A}} = \frac{\partial \underset{\sim}{\boldsymbol{A}}}{\partial x_l} \times \underline{\boldsymbol{e}}_l = A_{ik,l}\underline{\boldsymbol{e}}_i \otimes (\underline{\boldsymbol{e}}_k \times \underline{\boldsymbol{e}}_l) = \epsilon_{jkl} A_{ik,l}\underline{\boldsymbol{e}}_i \otimes \underline{\boldsymbol{e}}_j \tag{1}$$

in a Cartesian orthonormal coordinate system $(\underline{\boldsymbol{e}}_1, \underline{\boldsymbol{e}}_2, \underline{\boldsymbol{e}}_3)$.

2 Enhanced crystal plasticity models

2.1 Micromorphic crystal plasticity (Microcurl)

This model introduces additional degrees of freedom in the spirit of Eringen's micromorphic approach. Details of the model were presented in [20], and the necessary equations are recalled here. The model includes a plastic microdeformation variable, $\underset{\sim}{\boldsymbol{\chi}}^p$, as a second-rank generally non-symmetric tensor. The components of $\underset{\sim}{\boldsymbol{\chi}}^p$ are treated as independent degrees of freedom (DOF) of the material point, in addition to the usual displacement vector $\underline{\boldsymbol{u}}$:

$$DOF = \{\underline{\boldsymbol{u}}, \underset{\sim}{\boldsymbol{\chi}}^p\} \tag{2}$$

The model assumes that the microdeformation rate and its curl part $\underset{\sim}{\boldsymbol{\Gamma}}_\chi = \operatorname{curl} \underset{\sim}{\boldsymbol{\chi}}^p$ play a role in the power density of internal forces:

$$p^{(i)} = \underset{\sim}{\boldsymbol{\sigma}} : \dot{\underset{\sim}{\boldsymbol{H}}} + \underset{\sim}{\boldsymbol{s}} : \dot{\underset{\sim}{\boldsymbol{\chi}}}^p + \underset{\sim}{\boldsymbol{M}} : \operatorname{curl} \dot{\underset{\sim}{\boldsymbol{\chi}}}^p \tag{3}$$

where $\underset{\sim}{\boldsymbol{\sigma}}$, $\underset{\sim}{\boldsymbol{H}} = \operatorname{grad} \underline{\boldsymbol{u}}$, $\underset{\sim}{\boldsymbol{s}}$ and $\underset{\sim}{\boldsymbol{M}}$ are the Cauchy stress tensor, the deformation tensor, the relative stress tensor and the double stress tensor, respectively. The generalized stress tensors fulfill the two following balance equations:

$$\operatorname{div} \underset{\sim}{\boldsymbol{\sigma}} = 0, \quad \operatorname{curl} \underset{\sim}{\boldsymbol{M}} + \underset{\sim}{\boldsymbol{s}} = 0 \tag{4}$$

with the corresponding boundary conditions:

$$\underline{\boldsymbol{t}} = \underset{\sim}{\boldsymbol{\sigma}} \times \underline{\boldsymbol{n}}, \quad \underline{\boldsymbol{m}} = \underset{\sim}{\boldsymbol{M}} \times \underline{\underline{\boldsymbol{\epsilon}}} \times \underline{\boldsymbol{n}} \tag{5}$$

where $\underline{\boldsymbol{t}}$ and $\underline{\boldsymbol{m}}$ are simple and double tractions at the boundary, $\underline{\boldsymbol{n}}$ is the surface normal vector and $\underline{\underline{\boldsymbol{\epsilon}}}$ is the Levi-Civita permutation tensor.

The total deformation is split as usual into elastic and plastic parts:

$$\underset{\sim}{\boldsymbol{H}} = \underset{\sim}{\boldsymbol{H}}^e + \underset{\sim}{\boldsymbol{H}}^p \tag{6}$$

The elastic and plastic strain tensors are defined as:

$$\underset{\sim}{\boldsymbol{\varepsilon}}^e = \frac{1}{2}(\underset{\sim}{\boldsymbol{H}}^e + \underset{\sim}{\boldsymbol{H}}^{eT}), \quad \underset{\sim}{\boldsymbol{\varepsilon}}^p = \frac{1}{2}(\underset{\sim}{\boldsymbol{H}}^p + \underset{\sim}{\boldsymbol{H}}^{pT}) \tag{7}$$

The Helmholtz free energy function of the material is assumed to have the following arguments regarded as state variables:

$$\Psi(\underset{\sim}{\boldsymbol{\varepsilon}}^e, \underset{\sim}{\boldsymbol{e}}^p = \underset{\sim}{\boldsymbol{H}}^p - \underset{\sim}{\boldsymbol{\chi}}^p, \underset{\sim}{\boldsymbol{\Gamma}}_\chi = \operatorname{curl} \underset{\sim}{\boldsymbol{\chi}}^p) \tag{8}$$

where $\underset{\sim}{\boldsymbol{e}}^p$ is called the relative plastic deformation and measures the difference between plastic deformation ($\underset{\sim}{\boldsymbol{H}}^p$) and the plastic microdeformation ($\underset{\sim}{\boldsymbol{\chi}}^p$).

When the internal constraint $\underset{\sim}{\boldsymbol{e}}^p \equiv 0$ is enforced, the microdeformation then coincides with the plastic deformation and its curl is directly related to the dislocation density tensor [50]:

$$\underset{\sim}{\boldsymbol{\Gamma}}_{\chi} = \operatorname{curl} \underset{\sim}{\boldsymbol{\chi}}^p \equiv \operatorname{curl} \underset{\sim}{\boldsymbol{H}}^p \tag{9}$$

The strain gradient plasticity model as developed by Gurtin [37] and Svendsen [62] is therefore retrieved as a limit case of the micromorphic model as discussed in [20].
The reduced entropy inequality reads

$$\left(\underset{\sim}{\boldsymbol{\sigma}} - \rho\frac{\partial\psi}{\partial\underset{\sim}{\boldsymbol{\varepsilon}}^e}\right) : \dot{\underset{\sim}{\boldsymbol{\varepsilon}}}^e - \left(\underset{\sim}{\boldsymbol{s}} + \rho\frac{\partial\psi}{\partial\underset{\sim}{\boldsymbol{e}}^p}\right) : \dot{\underset{\sim}{\boldsymbol{e}}}^p + \left(\underset{\sim}{\boldsymbol{M}} - \rho\frac{\partial\psi}{\partial\underset{\sim}{\boldsymbol{\Gamma}}_{\chi}}\right) : \dot{\underset{\sim}{\boldsymbol{\Gamma}}}_{\chi} + (\underset{\sim}{\boldsymbol{\sigma}} + \underset{\sim}{\boldsymbol{s}}) : \dot{\underset{\sim}{\boldsymbol{H}}}^p \geq 0 \tag{10}$$

The following state laws are adopted.

$$\underset{\sim}{\boldsymbol{\sigma}} = \rho\frac{\partial\psi^e}{\partial\underset{\sim}{\boldsymbol{\varepsilon}}}\ ,\ \underset{\sim}{\boldsymbol{s}} = -\rho\frac{\partial\psi}{\partial\underset{\sim}{\boldsymbol{e}}^p},\ \underset{\sim}{\boldsymbol{M}} = \rho\frac{\partial\psi}{\partial\underset{\sim}{\boldsymbol{\Gamma}}_{\chi}} \tag{11}$$

In particular, it is assumed that the micromorphic dislocation density tensor $\underset{\sim}{\boldsymbol{\Gamma}}_{\chi}$ contributes only to the storage of energy and not to dissipation; see [32]. Linear relationships are then chosen:

$$\underset{\sim}{\boldsymbol{\sigma}} = \underset{\sim}{\boldsymbol{\Lambda}} : \underset{\sim}{\boldsymbol{\varepsilon}}^e,\ \underset{\sim}{\boldsymbol{s}} = -H_{\chi}\underset{\sim}{\boldsymbol{e}}^p,\ \underset{\sim}{\boldsymbol{M}} = A\underset{\sim}{\boldsymbol{\Gamma}}_{\chi} \tag{12}$$

where H_{χ} and A are generalized plastic moduli. They represent the two additional parameters introduced in the theory in comparison with standard continuum crystal plasticity. These parameters are associated with an intrinsic length scale defined as

$$l_{\text{Microcurl}} = \sqrt{\frac{A}{H_{\chi}}} \tag{13}$$

that naturally arises in the analytical solutions of some boundary value problems.
As a result, the residual intrinsic dissipation rate becomes

$$D = (\underset{\sim}{\boldsymbol{\sigma}} + \underset{\sim}{\boldsymbol{s}}) : \dot{\underset{\sim}{\boldsymbol{H}}}^p \geq 0 \tag{14}$$

The difference compared to the usual plastic power is the contribution of the relative stress $\underset{\sim}{\boldsymbol{s}}$. The flow rule can be derived from a viscoplastic potential $\Omega(\underset{\sim}{\boldsymbol{\sigma}} + \underset{\sim}{\boldsymbol{s}})$, which is a function of the effective stress $\underset{\sim}{\boldsymbol{\sigma}} + \underset{\sim}{\boldsymbol{s}}$ that intervenes in the dissipation rate in Eq. (14):

$$\dot{\underset{\sim}{\boldsymbol{H}}}^p = \frac{\partial\Omega}{\partial(\underset{\sim}{\boldsymbol{\sigma}} + \underset{\sim}{\boldsymbol{s}})} \tag{15}$$

For crystal plasticity with a single slip system, the plastic deformation rate, $\dot{\underset{\sim}{\boldsymbol{H}}}^p$, is given by

$$\dot{\underset{\sim}{\boldsymbol{H}}}^p = \dot{\gamma}\underline{\boldsymbol{\ell}} \otimes \underline{\boldsymbol{n}} \tag{16}$$

where $\underline{\boldsymbol{\ell}}$ is the slip direction and $\underline{\boldsymbol{n}}$ the normal vector to the slip plane.
A generalized Schmid criterion is proposed in the form:

$$|\tau + \underset{\sim}{\boldsymbol{s}} : (\underline{\boldsymbol{\ell}} \otimes \underline{\boldsymbol{n}})| = \tau_c \tag{17}$$

where τ_c is the critical resolved shear stress. The classical resolved Schmid stress is $\tau = \underset{\sim}{\boldsymbol{\sigma}} : (\underline{\boldsymbol{\ell}} \otimes \underline{\boldsymbol{n}})$.

The contribution in the yield condition (17)

$$\underset{\sim}{\boldsymbol{s}} : (\underline{\boldsymbol{\ell}} \otimes \underline{\boldsymbol{n}}) = -\operatorname{curl} \underset{\sim}{\boldsymbol{M}} : (\underline{\boldsymbol{\ell}} \otimes \underline{\boldsymbol{n}}) = -A\operatorname{curl} \underset{\sim}{\boldsymbol{\Gamma}}_{\chi} : (\underline{\boldsymbol{\ell}} \otimes \underline{\boldsymbol{n}}) \tag{18}$$

represents a size-dependent kinematic hardening component which is responsible for the size-dependent hardening effects described in the sequel of the paper [20,32,69].

2.2 FDM model

The dislocation density tensor or GND tensor also is the main ingredient of the FDM model according to [55,63,64]. The evolution of GNDs is evaluated by Mura's transport equation:

$$\dot{\underset{\sim}{\boldsymbol{\alpha}}} = -\text{curl}\, \dot{\underset{\sim}{\boldsymbol{H}}}^{p} \tag{19}$$

where $\underset{\sim}{\boldsymbol{\alpha}}$ and $\underset{\sim}{\boldsymbol{H}}^{p}$ are the Nye tensor induced by GND and the plastic deformation tensor as in the previous model, respectively. The plastic deformation rate is split into two contributions:

$$\dot{\underset{\sim}{\boldsymbol{H}}}^{p} = \underset{\sim}{\boldsymbol{L}}_{p} + \underset{\sim}{\boldsymbol{\alpha}} \times \underline{\boldsymbol{v}} \tag{20}$$

where $\underline{\boldsymbol{v}}$ is the velocity vector of mobile dislocations. The additional plastic distortion rate $\underset{\sim}{\boldsymbol{L}}_{p}$ accounts for plastic deformation due to SSD only. The second term in Eq. (20) represents additional plastic distortion due to the Nye tensor (GND contribution).

For instance, edge GNDs moving along the axis 1 direction are related to the component α_{12} of Nye's tensor ($v_1 = -v\frac{\alpha_{12}}{|\alpha_{12}|}$). When inserted in Eq. (20), their contribution to plastic deformation rate is

$$\dot{H}^{p}_{13} = \rho_{\text{SSD,M}} b v - \alpha_{12} v_1 \tag{21}$$

where $\rho_{\text{SSD,M}}$ is the moving SSD density. The velocity of dislocations v is obtained by the Arrhenius mobility equation:

$$v = v_0 \exp\frac{-\Delta G}{kT} \exp\frac{V(\tau - \tau_c)}{kT} \tag{22}$$

where V is the activation volume depending on material behavior and τ and τ_c, respectively, are the resolved shear stress and the critical resolved shear stress. The Taylor relation is used:

$$\tau_c = 0.3\mu b\sqrt{\rho_{\text{SSD,F}}} \tag{23}$$

where μ is the shear modulus and $\rho_{\text{SSD,F}}$ the forest SSD density.

Finally, the density $\rho_{\text{SSD,F}}$ is calculated by the extension of Kocks–Mecking law with three parameters (k_{SSD}, f and k_{GND}). In the previous case of single slip with edge dislocations, we have:

$$\dot{\rho}_{\text{SSD,F}} = \left(\frac{k_{\text{SSD}}}{b}\sqrt{\rho_{\text{SSD,F}}} - f\rho_{\text{SSD,F}} + k_{\text{GND}}\left|\frac{\alpha}{b}\right|\right)|\dot{H}^{p}_{13}| \tag{24}$$

where α is the norm of the dislocation density tensor and b the norm of the Burgers vector. Estimations of the material parameters for single-crystal copper can be found in [63].

3 Formulation of the problem and analytical expressions

3.1 The three considered physical situations

Figure 1 provides a schematic description of the three different physical situations considered for the DDD simulations. The simulation volume is a channel with height h and depth w set to 10 μm. The channel width s is chosen to vary from 1 to 5 μm so as to analyze the channel size effect. Because top and bottom faces of the channel are treated as periodic boundaries, the simulation volume represents an infinite strip along the global Z direction. The other four faces, perpendicular to the X and Y axes, are treated as boundaries impenetrable to dislocations.

One single slip system or two slip systems are embedded in the channel space. In the single slip case, the slip planes are perpendicular to the boundary or inclined at an angle θ with respect to the global Y-axis (see Fig. 1a, b). In the double slip case, the directions of width, depth and height of the channel are parallel to the [110], $[\bar{1}1\bar{1}]$ and $[\bar{1}12]$ orientations of a FCC crystal, respectively. The two slip systems correspond to the slip systems B4 ($\underline{\boldsymbol{b}} = [\bar{1}01], \underline{\boldsymbol{n}} = (111)$) and C1 ($\underline{\boldsymbol{b}} = [011], \underline{\boldsymbol{n}} = (\bar{1}\bar{1}1)$) according to Schmid–Boas notation (see Fig. 1c). The slip planes are taken equidistant with the interplane distance ranging from $l = 0.01$ μm to 10 μm. The limit case $l = 10$ μm corresponds to one single slip plane located at the center of the channel.

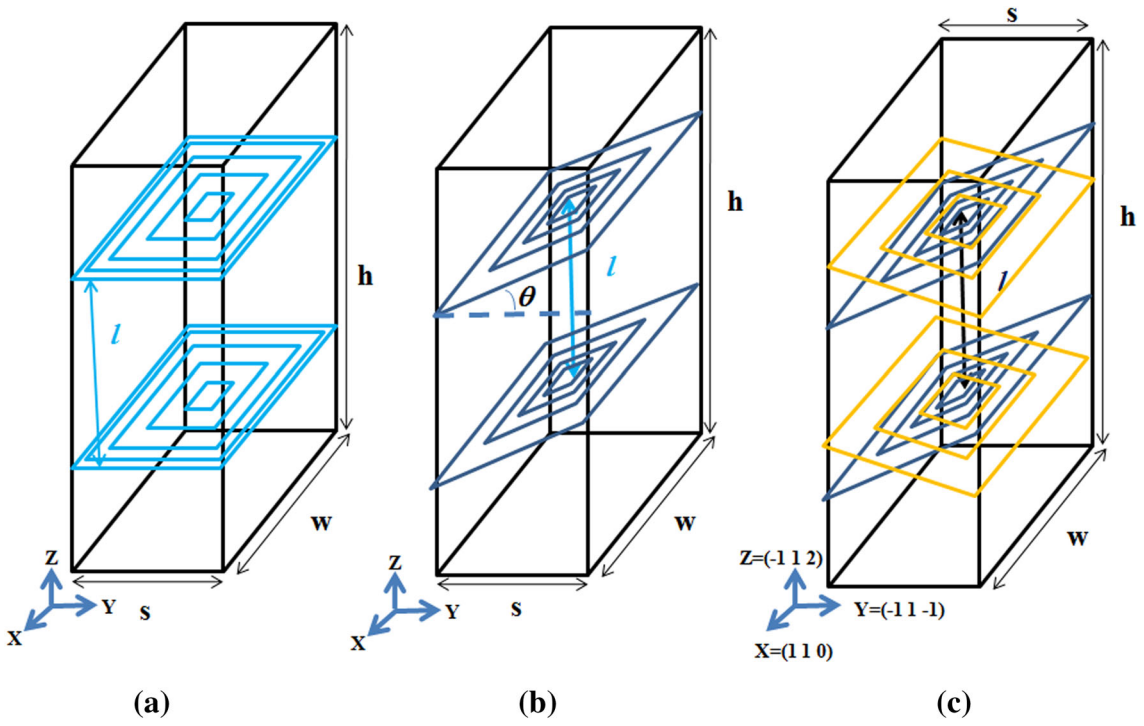

Fig. 1 Three physical situations considered in the work: **a** a channel with single slip system and slip planes orthogonal to the boundary; **b** a channel with a single slip system with slip planes inclined at a given angle θ with respect to Y-axis; **c** a channel with symmetric double slip systems, in which case the axes, X, Y and Z are parallel to $[\bar{1}1\bar{1}]$, [1 1 0] and $[\bar{1}12]$ orientations of the considered FCC crystal, respectively. The two slip systems correspond to systems B4 ($\underline{\boldsymbol{b}} = [\bar{1}01], \underline{\boldsymbol{n}} = (111)$) and C1 ($\underline{\boldsymbol{b}} = [011], \underline{\boldsymbol{n}} = (\bar{1}\bar{1}1)$) according to Schmid–Boas notation

Each slip plane is equipped with one Frank-Read source whose position is chosen randomly in the interval $-0.3s \leq X \leq 0.3s$ and $-0.3w \leq Y \leq 0.3w$, where s, w are defined in Fig. 1.

The elastic properties of the crystal are assumed to be isotropic ($\mu = 42\,\text{GPa}$, $\nu = 0.31$). A shear stress ($\tau = 0$ up to 600 MPa) is applied to the volume in the single slip system problem, while global shear or tension stress ($\sigma_{yz}, \sigma_{zz} = 0$ up to 600 MPa) is prescribed in the problem of double slip systems. The problem is kept as simple as possible to allow for direct comparison between the discrete and continuum approaches. In particular, *cross-slip is forbidden* and image forces at the impenetrable interfaces are not accounted for during the simulation.

Although the DDD simulation essentially is a dynamic problem (out of equilibrium) inducing instabilities and time dependency, it can also provide results corresponding to the quasi-static equilibrium state which is obtained by repeated calculation steps allowing for the relaxation of the dislocation structure under constant applied stress. Accordingly, the slip and GND distributions and stress–strain curves obtained by post-processing the DDD simulation results correspond here to a quasi-static state. Finally, the plastic hardening modulus is determined from the quasi-linear slope of the resulting stress–plastic strain curves.

Intrinsic lengths dominating the proposed DDD simulations must be identified. The distance between neighboring slip layers, l, plays a central role in the resulting size effects, for the two reasons schematically explained in Fig. 2. On the one hand, the intrinsic length l determines the amount of shear strain induced by the pile-up dislocations directly (Fig. 2a). The relative displacement between the top and bottom parts of the layer sheared by n_p dislocations with Burgers vector b:

$$\Delta u = n_p b \tag{25}$$

Then, the amount of slip between adjacent slip planes is determined by the relative displacement and the intrinsic length l, as shown in Fig. 2a:

$$\gamma = \frac{\Delta u}{l} = \frac{n_p b}{l} \tag{26}$$

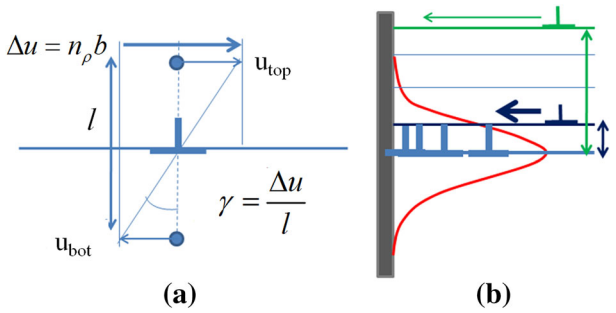

Fig. 2 Schematic explanation of the effect of the distance between slip layers, l in the stacked pile-up problem: **a** the amount of slip is calculated from the distance directly; **b** the shear stress field induced by a pile-up (*red line*) disturbs dislocations moving on neighboring slip planes. The amplitude of the perturbation depends on the distance l

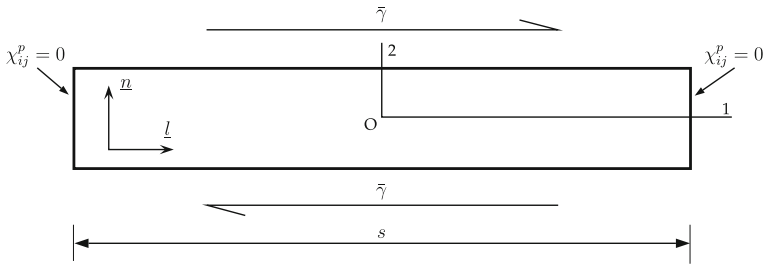

Fig. 3 Boundary value problem considered for the Microcurl model

On the other hand, the stress field induced by pile-ups restricts the motion of dislocations gliding on neighboring slip planes; see Fig. 2b.

The channel structure used in DDD simulations (Fig. 1) is simplified into a one-dimensional geometry in the continuum approach, because of invariance along the slip plane normal direction. Figure 3 depicts the geometry and boundary conditions of the problem based on the Microcurl model. The size of the channel, s, can be varied from *nm* to *mm* scale in the continuum model. The plastic microdeformation, $\underset{\sim}{\chi}^p$, is set to zero at the left and right boundaries so as to represent the condition of impenetrable interface in the continuum framework. Two kinds of slip systems are embedded in the model as in the DDD simulations. First, single slip is considered with an inclined slip plane ($\theta = 0$ to $90°$) and the other situation deals with double slip systems, B4 and C1, according to Schmid–Boas notation. The elastic properties for the channel are the same as those used in DDD simulation ($\mu = 42$ GPa, $\nu = 0.31$). The values of the micromorphic parameters, A and H_χ, are related by the intrinsic length, $l_{\text{Microcurl}}$, see Eq. (13), which can be varied from nm to μm scales. The attention is focused on the effects of channel size s and intrinsic length $l_{\text{Microcurl}}$ on slip distribution and related work-hardening. The results of the Microcurl model will be directly quantitatively compared with those from DDD simulations. Parameters A and H_χ will be identified from the results of DDD simulations.

Recently, one-dimensional FDM simulations were performed for a matrix-inclusion problem and for the channel problem with properties of aluminum by Taupin et al. [63,64]. They obtained the GND distributions in the matrix and channel, which are treated as numerical experiments for comparisons with DDD predictions of the present work. Complete details of parameters and simulation methods for the FDM are given in the two latter references. Although the existence of inclusions is not considered in our DDD problem and material properties between FDM and DDD simulations are not the same, it is worth comparing the two studies in terms of GND distributions at least qualitatively. In particular, the comparison will provide a physical description of the intrinsic length used in the FDM model, which had not been clearly identified yet.

3.2 Analytical expressions for hardening by multilayer pile-ups

Work-hardening induced by multilayer pile-ups can be derived from analytical expressions based on the theory of dislocations and the Microcurl model. Closed-form expressions are given here, the details of the derivation are to be found in [20,23,33], and the references quoted therein.

First of all, Mura has derived a simple solution for the work-hardening resulting from multilayer pile-ups [33]:

$$H_{\text{Mura}} = \frac{4}{\pi}\frac{\mu}{1-\nu}\frac{l}{s} \tag{27}$$

It is based on the solution of the single-dislocation pile-up model, thus neglecting the interaction between pile-ups. Accordingly, the solution should work reasonably only for the case of large values of l (see Fig. 2b).

On the other hand, Déprés [23] has suggested an alternative analytical expression to represent the additional work-hardening due to neighboring slip planes. The formula does not correspond to the exact solution of the problem of interacting pile-ups, but it is based on the assumption that the additional work-hardening decreases exponentially along the slip plane normal direction (see the red line in Fig. 2b):

$$H_{Déprés} = \frac{4}{\pi}\frac{\mu}{1-\nu}\frac{1+\exp\left(-k\frac{l}{s}\right)}{\left(\frac{s}{l}-2\right)\left(1-\exp\left(-k\frac{l}{s}\right)\right)+2} \tag{28}$$

where k is parameter accounting for additional work-hardening. The value $k = 2.0$ is found to reproduce at best the results of DDD simulations. The Déprés expression has two limit cases. Mura's solution is retrieved for large values of l [see Eq. (28)]. The other limit is derived for vanishing values of the pile-up spacing, l, or large values of channel width, s. It is remarkable that it is size-independent.

$$\lim_{\frac{l}{s}\to 0} H_{Déprés} = \frac{4}{\pi}\frac{\mu}{1-\nu}\frac{2}{k+2} \tag{29}$$

This limit case was not discussed in the literature yet and will be the result of the DDD simulations for closely interacting pile-ups.

The analytical expression of the overall work-hardening can also be derived using the Microcurl model, as done in [4,20]. It is obtained by averaging plastic slip in the channel and computing the stress. The result is

$$H_{\text{Microcurl}} = \frac{12AH_\chi}{12A + H_\chi s^2} \tag{30}$$

where H_χ and A are the material properties in the Microcurl model as defined in Eq. (12). Again, two limiting cases are of interest. When the channel size s goes to zero, the effective hardening modulus is equal to H_χ. Since $H_\chi \to +\infty$ corresponds to the case of strain gradient plasticity according to Gurtin's model, it is apparent that the hardening becomes infinite which is in accordance with Mura's formula. For large values of s, the overall hardening is found to vanish, which is in disagreement with (29). That is why an additional size-independent isotropic hardening component, not related to the micromorphic part of the model, is added in the Microcurl constitutive model, with plastic modulus called H_{offset}, in order to compensate the strengthening by neighboring slip planes:

$$H_{\text{Microcurl}} = \frac{12AH_\chi}{12A + H_\chi s^2} + H_{\text{offset}} \tag{31}$$

The value of H_{offset} is chosen equal to the value given by Eq. (29).

4 Results and discussion

4.1 Work-hardening by multilayer pile-ups

The DDD simulations of multilayer pile-ups predict dislocation structures induced by the applied stress. Figure 4a depicts dislocation multiplication produced by 200 MPa of shear loading along Y-direction, with channel width $s = 5$ μm and pile-up spacing $l = 2.5$ μm. The structure of the pile-ups in Fig. 4a is generated by Frank-Read sources on each slip plane, causing plastic slip. The piling-up dislocations are clearly visible on the four sides of the simulation box. Figure 4b depicts the overall stress–strain curves from DDD simulations with $s = 1$ μm and various intrinsic length values l ranging from 10 to 0.01 μm. Since the slip amount is proportional to the number of moving dislocations, it is directly related to the number of slip planes ($=\frac{h}{l}$)

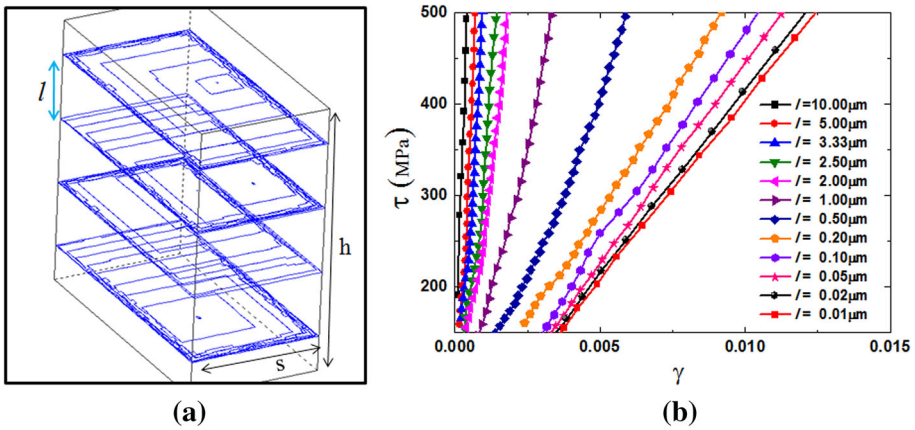

Fig. 4 **a** Dislocation structures induced by a prescribed shear stress $\tau = 200\,\text{MPa}$, for $s = 5$ μm and $l = 2.5$ μm. **b** Global stress–plastic slip curves for various intrinsic length values l and $s = 1$ μm

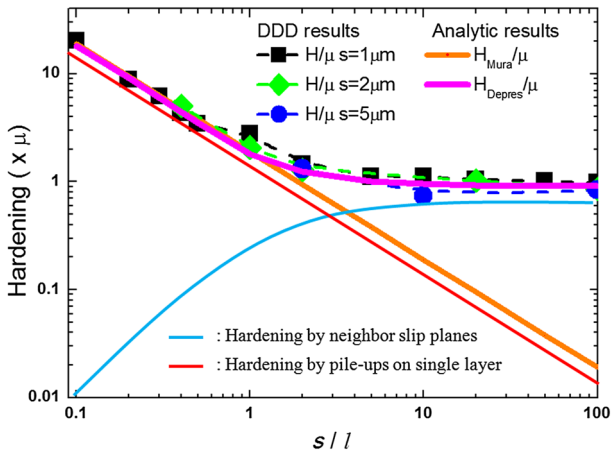

Fig. 5 Hardening modulus H versus s/l obtained from DDD simulations (H), Mura (H_{Mura}) and Déprés (H_{Depres}) formula. The *red line* corresponds to the case of single pile-up. Subtracting this *red line* from the DDD curve gives the *blue curve* highlighting the hardening induced by the interaction between pile-ups. SGP stands for Microcurl in the captions

in the channel. Accordingly, smaller l values lead to an increase in plastic slip at a given stress. However, plastic slip saturates because close enough pile-ups interact, thus hindering the movement of dislocations. The stress–overall plastic strain curves are clearly linear, the slope providing the work-hardening modulus, H.

The dependence of the relative effective hardening H/μ on the ratio s/l as predicted by the DDD simulations is shown in Fig. 5. DDD simulation results for various values of s and l lead to a master curve with respect to the ratio s/l. The DDD results are compared to the analytical expressions by Déprés and Mura [see Eqs. (27) and (28)]. There are two different regimes in the work-hardening evolution. When $s/l \ll 1$, both DDD and the two analytical expressions predict size-dependent work-hardening in the form of a power law with exponent 1. In contrast, for $s/l \gg 1$, the DDD simulations and the Déprés formula predict a saturating value of work-hardening. The failing of Mura's formula in that case is due to the absence of pile-up interaction in Mura's model.

The relation between work-hardening and the ratio s/l can be explained by two kinds of internal stresses impeding dislocation motion. On the one hand, moving dislocations on a slip plane are restricted by pile-ups on the same slip plane (red line in Fig. 5, called hardening by single-layer pile-ups). It gives a linear inverse relationship in agreement with Mura's formula. On the other hand, moving dislocations also feel the stresses induced by the pile-ups formed on neighboring slip planes (blue curve). The amplitude of the extra hindrance is closely related to the intrinsic length, l, as suggested in Fig. 2b. It can be ignored for small enough values of the s/l ratio, but it increases then with s/l and saturates for large enough values of this ratio. This behavior is well-captured by Déprés' heuristic formula, Eq. (29). Consequently, work-hardening is dominantly affected by

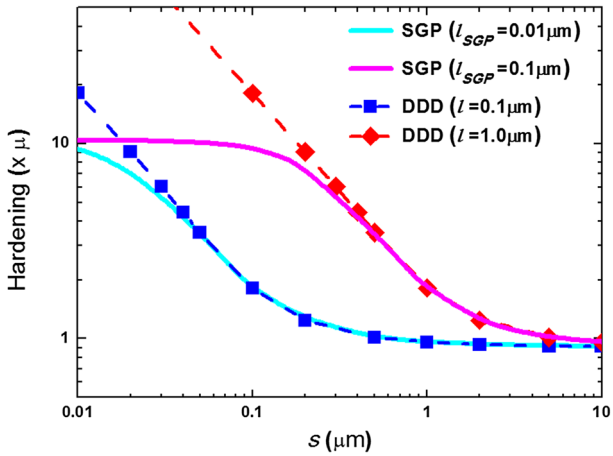

Fig. 6 Hardening modulus versus s in the range 0.01–10 μm from DDD simulations with $l = 0.1$ and 1.0 μm and according to the Microcurl model with $l_{\text{Microcurl}} = 0.01$ and 0.1 μm. The Microcurl model with appropriate intrinsic length, $l_{\text{Microcurl}} = 0.1 \times l$, reproduces the work-hardening from DDD simulations over a large range of s values. SGP stands for Microcurl in the captions

single-layer pile-up behavior in the size effect regime $s/l \ll 1$, while it is controlled by neighboring pile-ups in the size-insensitive regime $s/l \gg 1$.

The hardening modulus is plotted against the channel width s in Fig. 6 according to the DDD simulations and to the Microcurl model using two intrinsic lengths ($l_{\text{Microcurl}} = 0.01$ and 0.1 μm). The Microcurl model exactly reproduces the DDD results at least for sufficiently large values of s. It is found that the micromorphic intrinsic length corresponding to the best fitting of the DDD results scales with the pile-up spacing according to the following expression:

$$l_{\text{Microcurl}} = 0.1\, l \tag{32}$$

The Microcurl model reproduces the predictions of DDD except for the very small channel size regime. The size effect according to the Microcurl model saturates for vanishingly small values of s, as expected from Eq. (30). Parameter H_χ has also been calibrated so as to reproduce at best the evolution of the effective hardening modulus with s. A value of H_χ close to 10 μ was found to be satisfactory. The material parameter H_χ therefore settles the saturation value of the size-dependent hardening modulus, whereas the parameter $l_{\text{Microcurl}}$ controls the critical value of s for which saturation starts, as can be seen from Fig. 6. The physical relevance of the Microcurl model can be assessed based on the two following remarks. First, the material parameters A and H_χ allowing for a satisfactory description of the DDD results are independent of s, as it should be since s is a geometric characteristic of the boundary value problem. Second, they depend on l, the distance between dislocation sources, i.e., a material characteristics. In other words, these material parameters depend on the initial dislocation density and distribution.

The intrinsic length l of the DDD model controls the critical channel size separating the domain of size-dependent and size-independent hardening. If the channel size is smaller than the intrinsic length of DDD, size-sensitive work-hardening is observed whereas large channel sizes lead to size-independent behavior. On the other hand, the intrinsic length of the Microcurl model represents a transition boundary between size-dependent and saturated response. The saturation at nanoscales is reminiscent of grain size-independent behavior or even inverse grain size effects observed in nanograins [14,40]. This property of the model can be used in a phenomenological way, but the underlying physics does not correspond to the mechanisms responsible for inverse size effects, for instance related to grain boundary sliding or migration. Also, the continuum Microcurl model cannot be used at scales where dislocations are scarce since the continuum concept of crystal plasticity breaks down.

4.2 Effect of slip plane inclination

The effect of the inclination of slip planes with respect to the interfaces is now investigated using DDD and Microcurl simulations. Inclination of the slip plane is characterized by the angle θ taking the value $\theta = 0$ in the

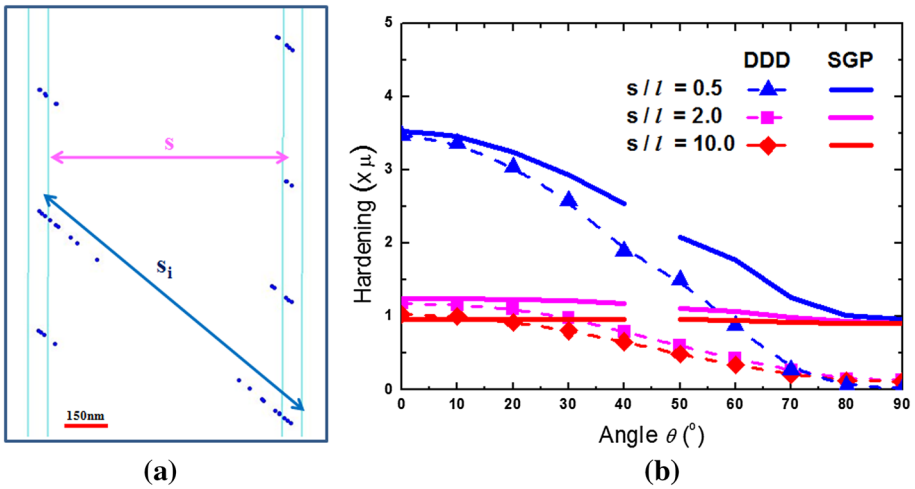

Fig. 7 **a** Two-dimensional dislocation structure of pile-ups on inclined slip planes for $s = 1$ μm, $l = 0.5$ μm and $\theta = 40°$. The inclined angle increases the distance between two-ended pile-ups, s_i. **b** Work-hardening versus inclined angles ($\theta = 0°$–$90°$) obtained from DDD and Microcurl simulations. SGP stands for Microcurl in the captions

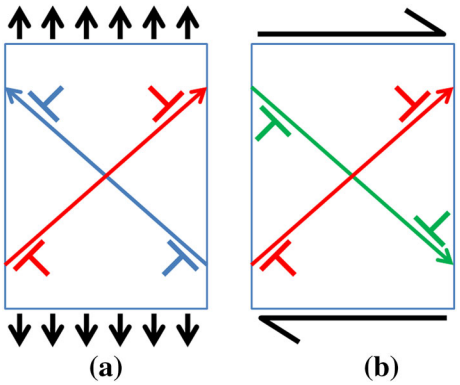

Fig. 8 Schematic diagram for activation of double slip systems according to loading conditions: **a** tensile loading activates both slip systems along positive directions; **b** shear loading induces opposite glide on the green slip system

previous case of horizontal pile-ups; see Fig. 1. Since the distance s_i between the two ends of pile-ups on an inclined slip plane increases with the inclination angle θ, as shown in Fig. 7a, increasing slip plane inclination causes a decrease in the observed work-hardening. In the limit case $\theta = 90°$ ($s_i = \infty$), the slip plane is parallel to the interfaces so that unlimited slip can occur and that no pile-up can form. Work-hardening vanishes in that case. Figure 7b shows the hardening modulus versus the inclination angle, θ, for both DDD and Microcurl simulations and three different s/l ratios. The same material parameters of the Microcurl model are used as identified in the previous $\theta = 0$ case, especially the relation (32) still holds. It is clearly visible that work-hardening predicted by DDD simulations monotonically decreases when the inclination angle increases from high values at $\theta = 0$ and $s/l = 0.5$ to almost zero for $\theta = 90°$. The Microcurl model predicts the same trend. The existence of the residual hardening for $\theta = 90°$ is an artifact of the introduction of the isotropic hardening component H_{offset} in Eq. (31). This interaction hardening component between neighboring pile-ups is poorly described in that way and should be progressively canceled when θ increases since the configuration leads less and less to such interaction effects. The proper modeling of this effect remains to be worked on. In contrast, the decreasing orientation-dependent internal stress induced by the pile-ups is satisfactorily reproduced by the Microcurl model. Both DDD and Microcurl model with the smallest ratio provide decreasing work-hardening due to increase in the angles. Simulations for the smallest ratio $s/l = 0.5$ display a significant size effect reproduced by the Microcurl model. In contrast, for the large value $s/l = 10$, strengthening by neighboring pile-ups becomes the dominant hardening mechanism.

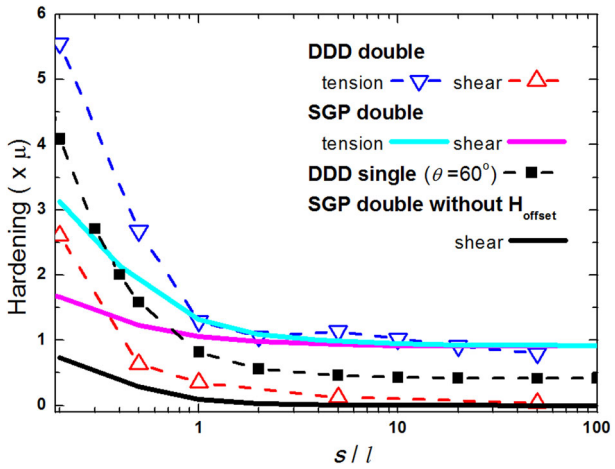

Fig. 9 Hardening modulus versus s/l due to double slip in a channel, as obtained from DDD and Microcurl simulations (with and without the additional component H_{offset}) under tension and shear loading conditions. Work-hardening for a single slip system inclined at $\theta = 60°$ is also presented for comparison. SGP stands for Microcurl in the captions

4.3 Double slip pile-ups

Double slip is now considered following the configuration of Fig. 1c showing the slip planes corresponding to the slip systems B4 and C1. The figure also shows the crystallographic orientation of the channel, with the axes Y and Z, respectively, parallel to $[\bar{1}1\bar{1}]$ and $[\bar{1}12]$. The considered loading conditions are shear in the YZ plane, in the Y direction, and tension along Z. Both lead to symmetric double slip in the channel.

Tension loading along Z triggers the activation of B4 and C1 slip systems in the positive directions indicated in Fig. 8a, where the red and blue lines correspond to B4 and C1 slip planes, respectively, and the arrows represent the activated slip direction. On the contrary, shear loading (σ_{XZ}) induces the activation of C1 in the opposite direction and B4 in the same direction as in tension (green line in Fig. 8b).

The results of DDD simulations are given in Fig. 9 in terms of the evolution of the observed overall hardening modulus H with respect to relative channel size. They are compared to predictions of the Microcurl model with and without consideration of the additional modulus, H_{offset}. The work-hardening obtained from DDD simulations for a single slip system with an inclination angle, $\theta = 60°$, is also depicted as a reference.

DDD simulations with double slip systems under tension loading lead to about twice more strain-hardening than in the single slip case, especially for $s/l > 1$ regime. In contrast, the case of shear loading exhibits significant less work-hardening, almost no hardening at all for large values of s/l. The Microcurl model accurately reproduces this special feature, at least when the additional hardening component H_{offset} is canceled. However, it accounts for the difference in hardening for tension and shear only for small values of s/l. This indicates that the hardening produced by the interaction of neighboring pile-ups depends on the multislip configurations induced by different loading conditions. The simple form of the Microcurl model cannot account for this effect.

Multislip interaction is described in the Microcurl model in an indirect way in the kinematic hardening component (18) where the overall couple stress tensor $\underset{\sim}{\boldsymbol{M}}$ and the micromorphic curvature $\underset{\sim}{\boldsymbol{\Gamma}}_{\chi}$ integrate the influence of all slip systems and not only that of the current one. As can be seen from Eq. (18), the size-dependent kinematic hardening is the projection of the couple stress tensor on the orientation tensor of the slip system. However, this simple model is apparently not sufficient to capture all the effects predicted by DDD simulations for double slip in tension and shear.

4.4 Plastic slip and GND distributions

The plastic strain is computed based on the swept area by dislocations in the elementary boxes of the discrete simulation. The grid size in the present work was 0.05 μm [27]. The amount of plastic slip in the middle plane YZ, predicted by the DDD simulations, is averaged along the Z direction and plotted as a function of Y in Fig. 10 for two values of s/l, in the case of single slip under overall shear. The plastic slip distribution is found to be

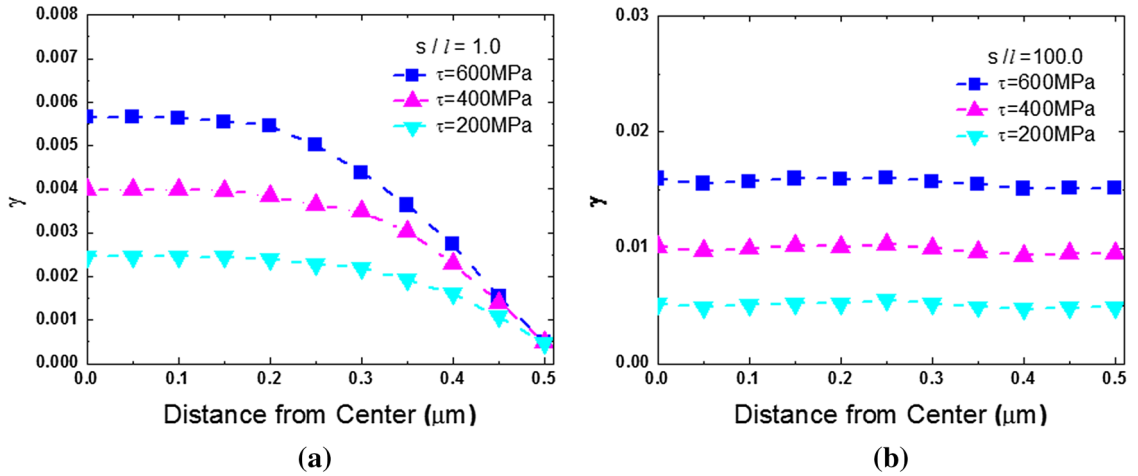

Fig. 10 Plastic slip distribution γ obtained by DDD simulations in the case of single slip under shear: **a** $s/l = 1.0$, **b** $s/l = 100.0$. SGP stands for Microcurl model in the caption

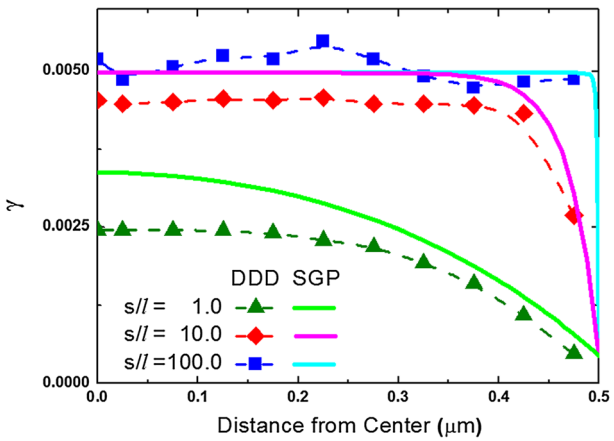

Fig. 11 Slip distributions obtained from DDD simulations with $l = 0.1$ μm and according to the Microcurl model with $l_{\text{Microcurl}} = 0.01$ μm, in the case of simple glide and 200 MPa applied shear stress

almost homogeneous for large channel widths. In contrast, slip is non-homogeneous in narrow channels with a plateau in the middle of a channel and a linear decrease toward the channel ends where slip almost vanishes due to the existence of impenetrable interfaces. Increasing the applied stress shortens the plateau zone and therefore increases the non-homogeneous character of slip distribution.

The previous DDD results are compared with the predictions of the Microcurl model in Fig. 11 for the same applied stress level of 200 MPa and three different values of the ratio $s/l = 1.0, 10.0, 100.0$. Note that the Microcurl simulation is performed with $s = 1$ μm of channel width and the appropriate internal length ($l_{\text{Microcurl}} = 0.1 \times l$). The figure shows that the Microcurl model can reproduce the results of DDD simulations quite accurately for the three ratios. In the presence of the additional hardening component H_{offset}, the analytical solution for the Microcurl model provides a cosh-profile of plastic slip explaining the plateau-like distribution in the middle of the channel [4].

The DDD results can also be interpreted in terms of dislocation densities by proper averaging over a small box around each material point, with the indicated grid size of 0.05 μm. In the case of single slip under shear, this local density mainly corresponds to that of GNDs. Figure 12 shows dislocation density distributions from DDD simulation for various ratios s/l and for an applied shear stress of 600 MPa. High values of s/l are associated with strongly localized GND density close to the boundary. For instance, the ratio $s/l = 100$ allows for a high concentration of GNDs only at the boundary. Decreasing the ratio causes the maximum GND density to decrease and the size of GND rich zone to extend (see Fig. 12a). Note that in the size-dependent regime, decreasing further s/l leads to a decrease of maximum GND density but does not seem to affect the size of the

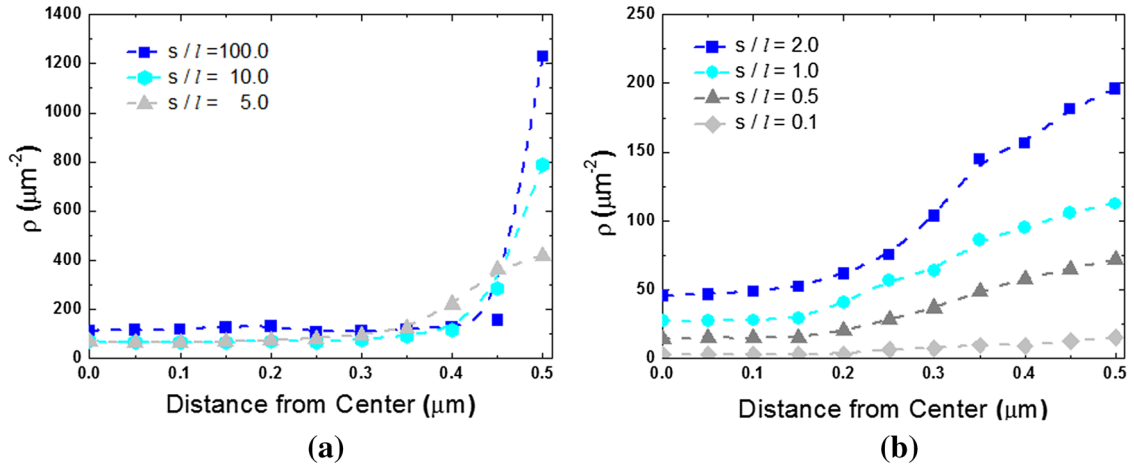

Fig. 12 Dislocation density distribution (GND) obtained by DDD simulations with various s/l ratios: **a** high values of s/l; **b** low values of s/l. Shear test under single slip conditions with 600 MPa prescribed stress

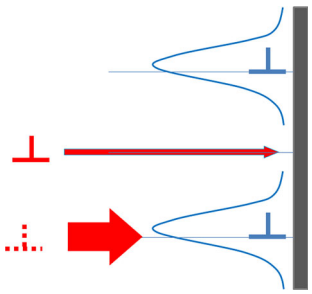

Fig. 13 Pile-ups form only once all slip planes are filled with dislocations, because the stress for dislocations to pile up (*red dot*) is always higher than for dislocations to fill empty slip planes (*red line*). The *blue curves* represent the stress field distribution due to dislocations close to the boundary

GND rich zone close to the boundary. This is probably related to the fact that each slip plane in the channel has a single source which does not interact with other sources.

The relationship between the s/l ratio and GND distribution can be explained by a simple schematic model. We assume that the pile-ups form only after all the active slip planes are filled with dislocations. This is because adding a new dislocation to build a pile-up requires higher stress than to fill an empty neighboring slip plane with fresh dislocations, as depicted schematically in Fig. 13. Therefore, small values of s/l allow for the formation of pile-ups from the beginning because few dislocations are needed to fill all the slip planes, as illustrated by Figs. 14a and 12b. On the other hand, large values of the s/l ratio represent many empty planes at the boundary, so that many dislocations will move to fill the empty slip planes instead of populating pile-ups; see Figs. 14b and 12a.

Recently, GND density distributions in laminate microstructures were also analyzed using one-dimensional FDM simulations by Taupin et al. [63,64]. Although details of the simulation conditions are somewhat different from the present ones, it is worth comparing the results of FDM and DDD. Figure 15a, b depicts GND distributions obtained by the FDM simulation [63] and DDD simulations, respectively. Note that the FDM simulation considers the mobile SSD density ($\rho_{\mathrm{SSD,M}}$) as an initial constant parameter. FDM predicts that the $\rho_{\mathrm{SSD,M}}$ is closely related to GND distribution. Very high mobile SSD density (green line) causes strong GND concentration at channel boundaries, while the GND rich zone extension increases for smaller SSD densities. These predictions are quite comparable to DDD results, as can be seen from Fig. 15b which shows the relationship between the s/l ratio and GND distribution in DDD simulations. The ratio s/l in the present DDD simulations plays a similar role as the mobile SSD density ($\rho_{\mathrm{SSD,M}}$) in the FDM model.

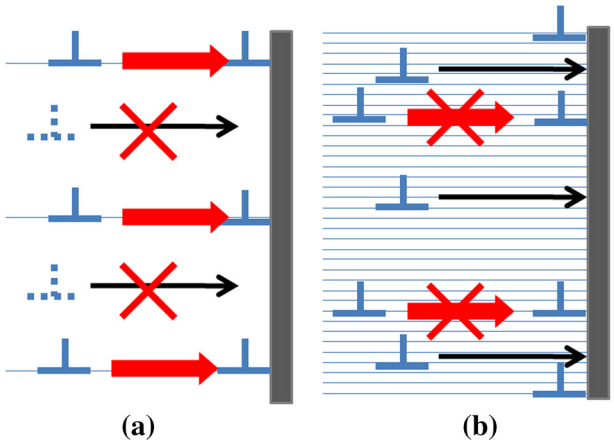

Fig. 14 Schematic explanation of the effect of the ratio s/l on GND distribution. **a** $s/l \ll 1$ case: few dislocations are needed to fill the slip planes. **b** $s/l \gg 1$ case: all dislocations are moving to fill empty slip planes

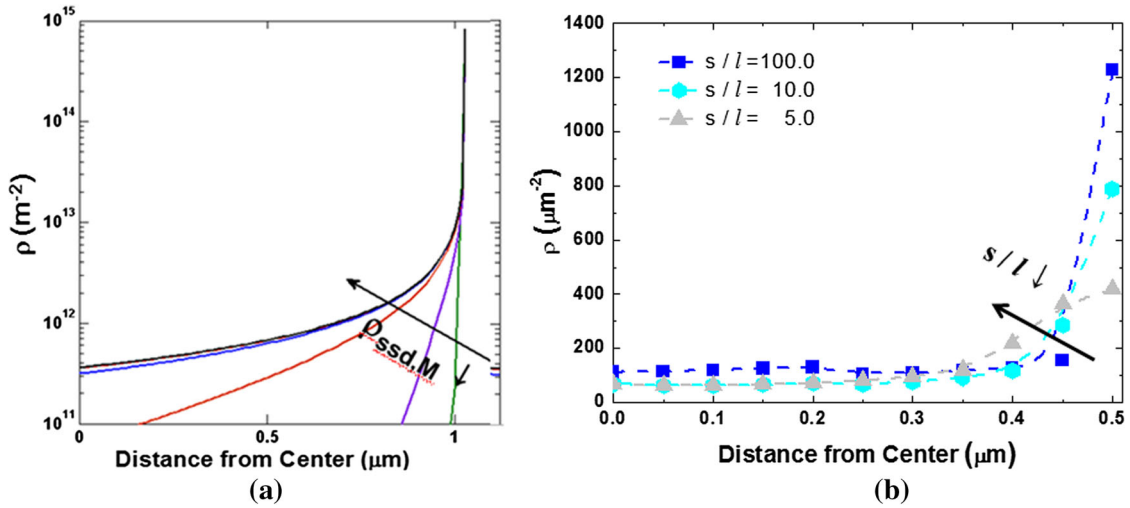

Fig. 15 **a** GND density distributions from FDM depending on the imposed mobile SSD density, from [63]; **b** GND density distributions from DDD simulations with s/l ratio

5 Conclusions

Multilayer pile-ups embedded in a channel microstructure with single or double slip systems were analyzed in terms of work-hardening, GND distribution and plastic slip distribution by means of DDD simulations and recent strain gradient plasticity models. The ratio of the channel width divided by the distance between dislocations sources, s/l, was shown to play a crucial role in the interpretation of DDD simulation results and was used in the discussion of the discrete and continuum simulation results. The main findings of this work are the following:

- High values of the ratio, s/l, lead to size-independent work-hardening and rather homogeneous plastic slip distribution for both discrete and continuum approaches. The DDD simulations show in particular that if l is very large, so that pile-ups do not interact with each other, and s sufficiently large, no overall hardening is observed macroscopically under shear loading for single and double slip.
- Small values of s/l are associated with size-dependent hardening and inhomogeneous distributions of slip, with a plateau and a steep decrease at channel boundaries.
- Size-independent hardening component was identified related to the interaction of neighboring pile-ups leading to remnant macroscopic work-hardening in tension and shear even for large values of the channel width.

– The formula (28) was proposed to represent the scaling law between the overall plastic modulus, channel width s and the intrinsic length l. It covers the size-dependent and size-independent regimes observed from DDD simulations. Mura's scaling law for non-interactive pile-ups is retrieved as a special case. The formula also incorporates the size-independent hardening component of interacting pile-ups.
– The micromorphic crystal plasticity model called Microcurl was shown to essentially reproduce the observed behavior for single slip and, to a lesser extent, double slip in a channel. The new parameters H_χ and A could be identified so as to reproduce quantitatively the DDD results. It was found that the intrinsic length $l_{\text{Microcurl}}$ scales with the material length l according to the formula (32). Accordingly, the Microcurl model adequately represents in a continuum framework the formation of pile-ups in crystal plasticity.
– The Microcurl model does not satisfactorily account for the interaction of pile-ups observed in the DDD simulations when l is small enough. Additional size-independent isotropic hardening associated with the parameter H_{offset} was introduced in an heuristic way to obtain good agreement in the case of single slip. This additional hardening component, however, was shown to differ for multislip and for different loading conditions, tension or shear, in the DDD simulations.
– The comparison between FDM and DDD simulations regarding GND distribution provided the relationship between two initial parameters, s/l for DDD and $\rho_{\text{SSD,M}}$ for FDM.

It was shown recently that standard strain gradient plasticity based on a linear relation between higher-order stresses and the dislocation density tensor, after [38], does not provide the proper scaling law for hardening in channels, namely $1/l^2$ instead of Mura's $1/l$ scaling law in accordance with DDD simulation results; see [20,31]. In contrast, micromorphic crystal plasticity possesses two material parameters that can be identified with DDD or experimental data to better reproduce the scaling behavior at least in a given range of channel sizes. An alternative approach is to adopt a nonlinear constitutive relationship in strain gradient plasticity as discussed in [32,69]. This corresponds to the choice of non-quadratic free energy potentials as recommended in [5,43,51,69].

The description of size-dependent hardening induced by multislip is a difficult issue in strain gradient and micromorphic plasticity. A direct interaction between slip systems is present in the Microcurl model but was shown to be insufficient to describe the DDD results for double slip. A similar discussion on the limitation of strain gradient plasticity modeling of GND interaction under multislip configurations can be found in [6] where DDD simulations are also used as reference results. The simplification induced by the consideration of the total dislocation density tensor instead of individual slip system contributions, and used in the Microcurl model, was recently discussed in [48]. More complex GND slip interaction laws are necessary for future developments.

The approach should be extended to the case of cross-slip events, neglected in the present work, in order to derive more realistic macroscopic laws. Comparisons between DDD simulations and generalized continuum models should be performed for cyclic plasticity following pioneering contributions in this field [24,25] and for the prediction of grain size effects in polycrystals including proper scaling laws and plastic slip fields inside the grains [21,22,45].

Acknowledgments This research was carried out under Project ANR-07-MAPR- 0023-04 CAT-SIZE Matériaux et Procédés. Financial support is gratefully acknowledged.

References

1. Acharya, A., Bassani, J.: Lattice incompatibility and a gradient theory of crystal plasticity. J. Mech. Phys. Solids **48**, 1565–1595 (2000)
2. Aifantis, E.: On the microstructural origin of certain inelastic models. J. Eng. Mater. Technol. **106**, 326–330 (1984)
3. Arsenlis, A., Parks, D.M.: Crystallographic aspects of geometrically-necessary and statistically stored dislocation density. Acta Mater. **47**, 1597–1611 (1999)
4. Aslan, O., Cordero, N.M., Gaubert, A., Forest, S.: Micromorphic approach to single crystal plasticity and damage. Int. J. Eng. Sci. **49**, 1311–1325 (2011)
5. Bardella, L., Panteghini, A.: Modelling the torsion of thin metal wires by distortion gradient plasticity. J. Mech. Phys. Solids **78**, 467–492 (2015)
6. Bardella, L., Segurado, J., Panteghini, A., Llorca, J.: Latent hardening size effects in small-scale plasticity. Modell. Simul. Mater. Sci. Eng. **21**(055), 009 (2013)
7. Baskaran, R., Akarapu, S., Mesarovic, S., Zbib, H.: Energies and distributions of dislocations in stacked pile-ups. Int. J. Solids Struct. **47**, 1144–1153 (2010a)

8. Baskaran, R., Akarapu, S., Mesarovic, S.D., Zbib, H.M.: Energies and distributions of dislocations in stacked pile-ups. Int. J. Solids Struct. **47**, 1144–1153 (2010b)
9. Bassani, J., Needleman, A., Van der Giessen, E.: Plastic flow in a composite: a comparison of nonlocal continuum and discrete dislocation predictions. Int. J. Solids Struct. **38**, 833–853 (2001)
10. Berbenni, S., Berveiller, M., Richeton, T.: Intra-granular plastic slip heterogeneities: discrete vs. mean field approaches. Int. J. Solids Struct. **45**, 4147–4172 (2008)
11. Bittencourt, E., Needleman, A., ME, G., Van der Giessen, E.: A comparison of nonlocal continuum and discrete dislocation plasticity predictions. J. Mech. Phys. Solids **51**, 281–310 (2003)
12. Busso, E., Meissonnier, F., O'Dowd, N.: Gradient-dependent deformation of two-phase single crystals. J. Mech. Phys. Solids **48**, 2333–2361 (2000)
13. Chang, H.J., Gaubert, A., Fivel, M., Berbenni, S., Bouaziz, O., Forest, S.: Analysis of particle induced dislocation structures using three-dimensional dislocation dynamics and strain gradient plasticity. Comput. Mater. Sci. **52**, 33–39 (2012)
14. Chokshi, A., Rosen, A., Karch, J., Gleiter, H.: On the validity of the Hall–Petch relationship in nanocrystalline materials. Scr. Metall. **23**, 1679–1683 (1989)
15. Chou, Y., Li, J.: Theory of dislocation pile-ups. In: Mura, T. (ed.) Mathematical Theory of Dislocations, pp. 116–177. ASME, New York (1969)
16. Cleveringa, H., Van der Giessen, E., Needleman, A.: Comparison of discrete dislocation and continuum plasticity predictions for a composite material. Acta Mater. **45**, 3163–3179 (1997)
17. Cleveringa, H., Van der Giessen, E., Needleman, A.: Discrete dislocation simulations and size dependent hardening in single slip. J. Phys. IV **8**, Pr4-83–Pr4-92 (1998)
18. Cleveringa, H., Van der Giessen, E., Needleman, A.: A discrete dislocation analysis of residual stresses in a composite material. Philos. Mag. A **79**, 863–920 (1999)
19. Collard, C., Favier, V., Berbenni, S., Berveiller, M.: Role of discrete intra-granular slip bands on the strain-hardening of polycrystals. Int. J. Plast. **26**, 310–328 (2010)
20. Cordero, N.M., Gaubert, A., Forest, S., Busso, E., Gallerneau, F., Kruch, S.: Size effects in generalised continuum crystal plasticity for two-phase laminates. J. Mech. Phys. Solids **58**, 1963–1994 (2010)
21. Cordero, N.M., Forest, S., Busso, E.P.: Generalised continuum modelling of grain size effects in polycrystals. C. R. Mec. **340**, 261–274 (2012a)
22. Cordero, N.M., Forest, S., Busso, E.P., Berbenni, S., Cherkaoui, M.: Grain size effects on plastic strain and dislocation density tensor fields in metal polycrystals. Comput. Mater. Sci. **52**, 7–13 (2012b)
23. Déprés, C.: Modélisation physique des stades précurseurs de l'endommagement en fatigue dans l'acier inoxydable 316L. Ph.D. thesis, Grenoble INP, France (2004)
24. Déprés, C., Robertson, C., Fivel, M.: Low-strain fatigue in 316l steel surface grains: a three-dimensional discrete dislocation dynamics modeling of the early cycles. Philos. Mag. **84**, 2257–2275 (2004)
25. Déprés, C., Reddy, G., Robertson, C., Fivel, M.: An extensive 3D dislocation dynamics investigation of stage-I fatigue crack propagation. Philos. Mag. **94**, 4115–4137 (2014)
26. Eshelby, J., Frank, F., Nabarro, F.: The equilibrium of linear arrays of dislocations. Philos. Mag. **7**, 351–364 (1951)
27. Déprés, C., Fivel, M.: An easy implementation of displacement calculations in 3D discrete dislocation dynamics codes. Philos. Mag. **94**, 3206–3214 (2014)
28. Fivel, M., Tabourot, L., Rauch, E., Canova, G.: Identification through mesoscopic simulations of macroscopic parameters of physically based constitutive equations for the plastic behaviour of fcc single crystals. J. Phys. IV **8**, 151–158 (1998)
29. Fleck, N., Hutchinson, J.: A phenomenological theory for strain gradient effects in plasticity. J. Mech. Phys. Solids **41**, 1825–1857 (1993)
30. Fleck, N., Hutchinson, J.: Strain gradient plasticity. Adv. Appl. Mech. **33**, 295–361 (1997)
31. Forest, S.: Questioning size effects as predicted by strain gradient plasticity. J. Mech. Behav. Mater. **22**, 101–110 (2013)
32. Forest, S., Guéninchault, N.: Inspection of free energy functions in gradient crystal plasticity. Acta. Mech. Sin. **29**, 763–772 (2013)
33. Forest, S., Sedláček, R.: Plastic slip distribution in two-phase laminate microstructures: dislocation-based vs. generalized-continuum approaches. Philos. Mag. A **83**, 245–276 (2003)
34. Gao, H., Huang, Y., Nix, W., Hutchinson, J.: Mechanism-based strain gradient plasticity—I. theory. J. Mech. Phys. Solids **47**, 1239–1263 (1999)
35. Geers, M., Peerlings, R., Peletier, M., Scardia, L.: Asymptotic behaviour of a pile-up of infinite walls of edge dislocations. Arch. Ration. Mech. Anal. **209**, 495–539 (2013)
36. Ghoniem, N., Sun, L.: Fast-sum method for the elastic field of three-dimensional dislocation ensembles. Phys. Rev. B **60**, 128–140 (1999)
37. Gurtin, M.: On the plasticity of single crystals: free energy, microforces, plastic-strain gradients. J. Mech. Phys. Solids **48**, 989–1036 (2000)
38. Gurtin, M.: A gradient theory of single-crystal viscoplasticity that accounts for geometrically necessary dislocations. J. Mech. Phys. Solids **50**, 5–32 (2002)
39. Hall, E.: The deformation and ageing of mild steel: III discussion of results. Proc. Phys. Soc. B **64**, 747–753 (1951)
40. Herzer, G.: Nanocrystalline soft-magnetic materials. Phys. Scr. **T49A**, 307–314 (1993)
41. Kim, G., Fivel, M., Lee, H.J., Shin, C., Han, H., Chang, H., Oh, K.: A discrete dislocation dynamics modeling for thermal fatigue of preferred oriented copper via patterns. Scr. Mater. **63**, 788–791 (2010)
42. Kochmann, D., Le, K.: Dislocation pile-ups in bicrystals within continuum dislocation theory. Int. J. Plast. **24**, 2125–2147 (2008)
43. Kooiman, M., Hütter, M., Geers, M.: Microscopically derived free energy of dislocations. J. Mech. Phys. Solids **78**, 186–209 (2015)
44. Kubin, L., Canova, G., Condat, M., Devincre, B., Pontikis, V., Bréchet, Y.: Dislocation microstructures and plastic flow: a 3D simulation. Solid State Phenom. **23 & 24**, 455–472 (1992)

45. Lefebvre, S., Devincre, B., Hoc, T.: Yield stress strengthening in ultrafine-grained metals: a two-dimensional simulation of dislocation dynamics. J. Mech. Phys. Solids **55**, 788–802 (2007)
46. Madec, R., Devincre, B., Kubin, L., Hoc, T., Rodney, D.: The role of collinear interaction in dislocation-induced hardening. Science **301**, 1879–1882 (2003)
47. Mesarovic, S., Baskaran, R., Panchenko, A.: Thermodynamic coarsening of dislocation mechanics and the size-dependent continuum crystal plasticity. J. Mech. Phys. Solids **58**, 311–329 (2010)
48. Mesarovic, S., Forest, S., Jaric, J.: Size-dependent energy in crystal plasticity and continuum dislocation models. Proc. R. Soc. A **471**(20140), 868 (2015)
49. Mughrabi, H.: Dislocation wall and cell structures and long-rang internal stresses in deformed metal crystals. Acta Metall. **31**, 1367–1379 (1983)
50. Nye, J.: Some geometrical relations in dislocated crystals. Acta Metall. **1**, 153–162 (1953)
51. Ohno, N., Okumura, D.: Higher-order stress and grain size effects due to self-energy of geometrically necessary dislocations. J. Mech. Phys. Solids **55**, 1879–1898 (2007)
52. Ortiz, M., Repetto, E., Stainier, L.: A theory of subgrain dislocation structures. J. Mech. Phys. Solids **48**, 2077–2114 (2000)
53. Petch, N.: The cleavage strength of polycrystals. J. Iron Steel Inst. **174**, 25–28 (1953)
54. Richeton, T., Berbenni, S.: Effect of heterogeneous elasticity coupled to plasticity on stresses and lattice rotation in bicrystals: a Field Dislocation Mechanics viewpoint. Eur. J. Mech. A Solids **37**, 231–247 (2013)
55. Roy, A., Acharya, A.: Finite element approximation of field dislocation mechanics. J. Mech. Phys. Solids **53**, 143–170 (2005)
56. Scardia, L., Peerlings, R., Peletier, M., Geers, M.: Mechanics of dislocation pile-ups: a unification of scaling regimes. J. Mech. Phys. Solids **70**, 42–61 (2014)
57. Schwartz, K.: Simulation of dislocations on the mesoscale: I. Methods and example. J. Appl. Phys. **85**, 108–119 (1999)
58. Scouwenaars, R., Seefeldt, M., Houtte, P.: The stress field of an array of parallel dislocation pile-ups: implications for grain boundary hardening and excess dislocation distributions. Acta Mater. **58**, 4344–4353 (2010)
59. Shin, C.S., Fivel, M.C., Verdier, M., Oh, K.H.: Dislocation-impenetrable precipitate interaction: a three-dimensional discrete dislocation dynamics analysis. Philos. Mag. **83**, 3691–3704 (2003)
60. Shu, J., Fleck, N., Van der Giessen, E., Needleman, A.: Boundary layers in constrained plastic flow: comparison of non local and discrete dislocation plasticity. J. Mech. Phys. Solids **49**, 1361–1395 (2001)
61. Šiška, F., Weygand, D., Forest, S., Gumbsch, P.: Comparison of mechanical behaviour of thin film simulated by discrete dislocation dynamics and continuum crystal plasticity. Comput. Mater. Sci. **45**, 793–799 (2009)
62. Svendsen, B.: Continuum thermodynamic models for crystal plasticity including the effects of geometrically-necessary dislocations. J. Mech. Phys. Solids **50**, 1297–1329 (2002)
63. Taupin, V., Berbenni, S., Fressengeas, C., Bouaziz, O.: On particle size effects: an internal length mean field approach using field dislocation mechanics. Acta Mater. **58**, 5532–5544 (2010)
64. Taupin, V., Berbenni, S., Fressengeas, C.: Size effects on the hardening of channel-type microstructures: a field dislocation mechanics-based approach. Acta Mater. **60**, 664–673 (2012)
65. Upadhyay, M., Capolungo, L., Taupin, V., Fressengeas, C.: Elastic constitutive laws for incompatible crystalline media: the contributions of dislocations, disclinations and G-disclinations. Philos. Mag. **93**, 794–832 (2012)
66. Weygand, D., Friedman, L., Van der Giessen, E., Needleman, A.: Discrete dislocation modeling in three-dimensional confined volumes. Mater. Sci. Eng. A **309–310**, 420–424 (2001)
67. Wulfinghoff, S., Böhlke, T.: Equivalent plastic strain gradient enhancement of single crystal plasticity: theory and numerics. Proc. R. Soc. A **468**, 2682–2703 (2012)
68. Wulfinghoff, S., Bayerschen, E., Böhlke, T.: A gradient plasticity grain boundary yield theory. Int. J. Plast. **51**, 33–46 (2013)
69. Wulfinghoff, S., Forest, S., Böhlke, T.: Logarithmic and rank-one defect energies in gradient crystal plasticity analytical and numerical 1D solutions. J. Mech. Phys. Solids **79**, 1–20 (2015)
70. Yefimov, S., Van der Giessen, E.: Multiple slip in a strain-gradient plasticity model motivated by a statistical-mechanics description of dislocations. Int. J. Solids Struct. **42**, 3375–3394 (2005)
71. Yefimov, S., Groma, I., Van der Giessen, E.: A comparison of a statistical-mechanics based plasticity model with discrete dislocation plasticity calculations. J. Mech. Phys. Solids **52**, 279–300 (2004)
72. Zbib, H., Rhee, M., Hirth, J.: On plastic deformation and the dynamics of 3D dislocations. Int. J. Mech. Sci. **40**, 113–127 (1998)